Altered patterns of global protein synthesis and translational fidelity in RPS15-mutated chronic lymphocytic leukemia

Gabriel Bretones, Miguel G. Álvarez, Javier R. Arango, David Rodríguez, Ferran Nadeu, Miguel A. Prado, Rafael Valdés-Mas, Diana A. Puente, Joao A. Paulo, Julio Delgado, Neus Villamor, Armando López-Guillermo, Daniel J. Finley, Steven P. Gygi, Elías Campo, Víctor Quesada and Carlos López-Otín

Supplemental Data

Supplemental Methods

Culture media, buffers and reagents.

I10F medium was composed of Iscove's Modified Dulbecco's Medium (IMDM, Gibco) supplemented with 10% (v/v) fetal bovine serum (FBS, Gibco). D10F medium was composed of Dubecco's Modified Eagle Medium (DMEM, Gibco) supplemented with 10% (v/v) fetal bovine serum (FBS, Gibco). Additionally, all media were supplemented with 1% (v/v) of 100X Antibiotic-Antimycotic (Gibco) and 1% (v/v) of 100X Penicillin-streptomycin-glutamine (Gibco). Transduced cells were selected with 10 µg/mL blasticidin S (Invitrogen) or 2 µg/mL puromycin (Sigma Aldrich) as indicated. 10 mg/mL cycloheximide (CHX, Sigma Aldrich),100 mM actinomycin D (ACTD, Sigma Aldrich), 100 mM ibrutinib (Santa Cruz, sc-483194), 10 mM sorafenib (Santa Cruz, sc-220125) and 10 mM fludarabine (Santa Cruz, sc-204755) stock solutions were prepared in dimethyl sulfoxide (DMSO, Sigma-Aldrich). 100 µM bortezomib (Santa Cruz Biotechnology) stock solution was prepared in 1X PBS. Stock solutions were directly added to the culture medium to obtain the final working concentrations. An equal volume of drug solvent (PBS or DMSO) was added to the control cells. For the immunoblotting experiments, the NP-40 lysis buffer contained 50 mM Tris-HCl pH 7.4, 150 mM NaCl, 10mM EDTA pH 8, and 1% (v/v) NP-40 (Sigma Aldrich). NP-40 lysis buffer was supplemented with complete protease inhibitor cocktail (Roche), as well as 20 mM NaF (Merck) and PhosSTOP

phosphatases inhibitor cocktail (Roche) before use. For SDS-PAGE, protein samples were mixed with 4X SDS-PAGE loading buffer containing 200 mM Tris HCl pH 6.8, 8% (w/v) sodium dodecyl sulfate (SDS), bromophenol blue (1 mg/mL), 40% (v/v) glycerol and 2% (v/v) β-mercaptoethanol (all from Sigma-Aldrich). TBST buffer contained 20 mM Tris-HCl pH 7.4, 150 mM NaCl and 0.05% (v/v) Tween-20 (Sigma-Aldrich). For Ribosome isolation experiments, the ribosome homogenization buffer contained 50 mM Tris-HCl, pH 7.5, 5 mM $MgCl_2$, 25 mM KCl, 0.25% (v/v) Triton X-100 and 0.2 M sucrose, and the sucrose cushion buffer was composed of 50 mM Tris-HCl, pH 7.5, 5 mM $MgCl_2$, 25 mM KCl, and 2 M sucrose. For immunoprecipitations, the Co-IP lysis buffer contained 50 mM Tris-HCl pH 8, 150 mM NaCl, 1.5 mM $MgCl_2$, 5 mM EDTA, 1 mM DTT, 1% (v/v) NP-40 and was supplemented with protease inhibitor cocktail (Roche) before use. The Co-IP washing buffer was composed of 50 mM Tris-HCl pH 8, 150 mM NaCl, 1.5 mM $MgCl_2$, 5 mM EDTA, 1 mM DTT and 0.1% (v/v) NP-40. For fluorescence microscopy and immunofluorescence experiments, cells were fixed in 4% PFA-solution containing 4% (v/v) formaldehyde (Merck) in 1X PBS, and stained with 1µg/mL pyronin Y (Sigma Aldrich) in 1X PBS.

DNA constructs and site-directed mutagenesis.

Full-length RPS15 transcript variant 1, and RPS15 variants P131S and S138F, cloned with an in-frame N-terminal DYKDDDDK tag in the pUC57 vector, were purchased from GeneScript. $RPS15^{wt}$, $RPS15^{P131S}$ and $RPS15^{S138F}$ were subcloned into a custom modified pEGFP-C3 vector (Clontech) to generate GFP-RPS15 constructs. Finally, GFP-RPS15 constructs were subcloned into pCDH-CMV-MCS-EF1-Puro lentiviral vector (Addgene) in which puromycin resistance was replaced with blasticidin resistance. pCDH-CMV-GFP-$RPS15^{G132S}$-EF1-Blast, pCDH-CMV-GFP-$RPS15^{G134R}$-EF1-Blast, pCDH-CMV-GFP-$RPS15^{T136A}$-EF1-Blast, pCDH-CMV-GFP-$RPS15^{H137Y}$-EF1-Blast, pCDH-CMV-GFP-$RPS15^{S139F}$-EF1-Blast and pCDH-CMV-GFP-$RPS15^{K145N}$-EF1-Blast lentiviral vectors were generated by site-directed mutagenesis of pCDH-CMV-GFP-$RPS15^{WT}$-EF1-Blast vector using the QuickChange XL site-directed mutagenesis kit (Stratagene) and the following oligonucleotides: 5´-GCATGGCCGGCCC**A**GCATCGGG GCCAC-3´ and 5´-GTGGCCCCGATGC**T**GGGCCGGCCATGC-3´ for the G132S variant; 5´-CCGGCCCGGCATC**A**GGGCCACCCACTC-3´ and 5´-GAGTGGGTGGCC C**T**GATGCCGGGCCGG-3´ for the G134R variant; 5´-CGGCATCGGGGCC**G**CCCA CTCCTCCCG-3´ and 5´-CGGGAGGAGTGGG**C**GGCCCCGATGCCG-3´ for the T136A variant; 5´-CATCGGGGCCACC**T**ACTCCTCCCGCTTC-3´ and 5´-GAAGCGGGAGGA

GT**A**GGTGGCCCCGATG-3´ for the H137Y variant; 5´-GGCCACCCACTCCT**T**CC GCTTCATCCCTCTC-3´ and 5´-GAGAGGGATGAAGCGG**A**AGGAGTGGGTGGCC-3´ for S139F variant; and 5´-GCTTCATCCCTCTCAA**T**TAACTCGAGGATCCGC-3´ and 5´-GCGGATCCTCGAGTTA**A**TTGAGAGGGATGAAGC-3´ for the K145N variant. The bicistronic reporter pCDNA3-RLuc-POLIRES-FLuc containing the poliovirus (POL) internal ribosome entry site (IRES) controlling the Firefly luciferase gene (FLuc) to monitor cap-independent translation, and the CMV promoter controlling the Renilla luciferase gene (RLuc) to monitor the cap-dependent translation, which have been previously described[1], were purchased from Addgene (Plasmid #45642). The pCI-6.20 vector expressing FLuc and RLuc fused by the short peptide P2A from porcine teschovirus-1 polyprotein, which has been previously described[2], was purchased from Addgene (Plasmid #41002). During the elongation, eukaryotic ribosomes fail to insert a peptide bond between the Gly and Pro residues of P2A yielding two separate polypeptides[3]. In addition, pCI.6.20-FLuc-K529N-A>**T/C** (AAA>AA**T**/**C**) vectors were generated by site-directed mutagenesis of pCI6.20 vector using the QuickChange XL site-directed mutagenesis kit (Stratagene) and the oligonucleotides 5´-GAAAGGTCTT ACCGGAAA**T**/**C**CTCGACGCAAGAAAAATC-3´ and 5´-GATTTTTCTTGCGTCGAG**A/G** TTTCCGGTAAGACCTTTC-3´. These plasmids carry the K529N variant which renders the firefly enzyme catalytically inactive[4-6]. Thus, ribosomes with a reduced ability to discriminate between cognate and near-cognate aminoacyl-tRNAs yield higher levels of firefly luminescence. pCI-6.20-RFfusion vector was generated by replacing P2A (EFGSGATNFSLLKQAGDVEENPGP) by the EFETGYRL fusion peptide in between the Firefly and Renilla genes of pCI-6.20 vector. Thus, we inserted in between EcoRI and BstBI restriction sites the hybridized oligonucleotides 5´-AATTCGAGACGGGATACCGT CTCATGACTT-3´ and 5´-CGAAGTCATGAGACGGTATCCCGTCTCG-3´, generating two new repeated and inverted BsmBI restriction sites. pCI-6.20-STOP1, pCI-6.20-STOP2 and pCI-6.20-STOP3 constructs were generated by inserting 5´-AATTCGAGAC GGGATA**A**CGTCTCA-3´ and 5´-GTCATGAGACG**T**TATCCCGTCTCG-3´, 5´-AATTCG AGACGGGATA**G**CGTCTCA-3´ and 5´-GTCATGAGACG**C**TATCCCGTCTCG-3 or 5´-AATTCGAGACGGGAT**GA**CGTCTCA-3´ and 5´-GTCATGAGACG**TC**ATCCCGTCTCG-3´ hybridized oligonucleotides, respectively, in between BsmBI restriction sites of the pCI-6.20-RFfusion vector. The LentiCRISPRv2, previously described[7], was purchased from Addgene (Plasmid #52961). LentiCRISPR-sgEMPTY(Ø) and LentiCRISPR-sgRNA-RPS15 vectors were generated by inserting 5´-CACCGGAGACGG GATACCGTCTCT-3´ and 5´-AAACAGAGACGGTATCCCGTCTCC-3´, or 5´-CACCGG CTGCATCAGCTGCTCGCTG-3´ and 5´-AAACCAGCGAGCAGCTGATGCAGCC-3´ hybridized oligonucleotides, respectively, in between BsmBI restriction sites of the

LentiCRISPRv2 vector. Lentiviral packaging plasmids psPAX2 (Plasmid #12260) and pMD2.G (Plasmid #12259) were purchased from Addgene. All constructs were sequenced and validated before experimental use.

Lentiviral preparation and transduction

Lentiviral vectors were transfected into HEK293T cells along with packaging plasmids psPAX2 and pMD2.G. 48 h post-transfection, supernatants were collected, filtered through a 0.45 µm filter, precipitated overnight with 1 volume of PEG-solution (20% Polyethylene glycol (PEG)-4000 in PBS) and concentrated by centrifugation at 4000 rpm. Virus titer was determined by transducing HEK293T cells with serial dilutions of concentrated viruses and visually assessing the percentage of GFP-expressing or antibiotic resistant cells. Cells were infected with the desired titer for 24 h with 0.8 µg/mL polybrene (Santa Cruz Biotechnology).

Proliferation and viability assays

For proliferation assays, three independent clones obtained from HEK293T cells stably expressing the different GFP-RPS15 constructs and transduced with the lentiCRISPRv2-empty (Ø) vector or the lentiCRISPRv2-sgRNA against endogenous *RPS15* locus were seeded into 96-well plates at a density of 10000 cells per well. Proliferation was monitored every day by measuring the conversion of a tetrazolium salt into formazan in metabolically active cells using the Cell Titer 96 Non-Radioactive proliferation kit (Promega). Formazan absorbance was measured at 570nm with a Varioskan Flash microplate reader (Thermo Scientific).

For viability assays, three independent HEK293T clones with partially or totally ablated endogenous *RPS15* were seeded into 96-well plates at a density of 20000 cells per well and treated with the indicated concentrations of ibrutinib (0-62,5 µM), sorafenib (0-62,5 µM) or fludarabine (0-512 µM) for 72 h in 96-well plates. Viability rates were measured with the Cell Titer 96 Non-Radioactive proliferation kit (Promega), in a Varioskan Flash microplate reader (Thermo Scientific) following the manufacturer's instructions. For the half maximal inhibitory concentration (IC50) determination, normalized absorbance values were fitted to a curve using the [Inhibitor] vs. normalized response (variable slope) non-linear regression equation and the least squares fitting method with GraphPad Prism 7.0 software.

Immunofluorescence microscopy analysis

HEK293T cells were fixed with a 4% PFA-solution, permeabilized with PBS-containing 0.5% Triton X-100 and blocked with PBS-containing 15% goat serum (Gibco), followed by an overnight incubation with rabbit anti-RPS15 or mouse anti-FLAG antibodies. Immunofluorescence was detected using Alexa Fluor 546 anti-rabbit or anti-mouse secondary antibodies (Invitrogen), respectively. For pyronin Y (PY) staining, coverslips were incubated with 1 µg/mL PY (Sigma Aldrich) in PBS for 5 min at room temperature and washed 3 times with 1%-PBS before mounting. The coverslips were mounted on slides using 4´,6-diamidino-2-phenylindole (DAPI)-containing Vectashield ProLong Gold antifade reagent (Invitrogen), and imaged in an Axiovert 200M microscope (Zeiss) equipped with 100X and 63X Plan-Apochromat objectives, an HBO mercury lamp and different fluorescent filter Sets for GFP, DAPI or Alexa Fluor 546 fluorescent dyes. 100X images were captured using an AxioCam MRm digital CCD camera and processed with the Zeiss AxioVision 4.7 software.

Library preparation and deep-targeted next generation sequencing (NGS)

Libraries were generated using the Access-Array system (Fluidigm) and sequenced in a MiSeq equipment (Illumina). Through this approach, the average sequencing coverage across the target region was 1715x (1764x and 1617x for exons 3 and 4, respectively), with 63% of the samples having >75% of the sequence at >100x. After bioinformatic analysis, synonymous variants and polymorphisms described in dbSNP142 with a European population frequency >1% (1000 Genomes Project database) were removed. Variants passing the preceding filter were considered somatic when they were truncating or annotated as such in COSMIC (v77, http://cancer.sanger.ac.uk/cosmic) or in our custom CLL database[8]. Variants not satisfying any of the previous criteria were analyzed in the germ line DNA of the patient. Among the somatic mutations reported in the validation cohort, all but two were verified by allele-specific PCR using the 5´-CCCGC TTCATCCCTCTCA/**T**-3´ as wild type/mutated forward primer and 5´-GGAGATGAGG GAAGCCAGAA-3´ as reverse primer or by a second independent round of NGS. The two mutations in which the verification step was not performed were present at high variant allele frequencies (VAF of 25% and 41%).

Bioinformatic workflow applied to the extended cohort.

The bioinformatic analysis was performed as previously described[9]. Briefly, raw reads were trimmed using Trimmomatic (v0.32)[10] and the specific primers removed using Flexbar (v2.5)[11]. Trimmed reads were mapped to the reference genome (GRCh37/hg19) using the Burrows-Wheeler Aligner–MEM algorithm (v0.7.10)[12]. GATK[13] base quality score recalibration and indel realignment was performed before variant calling by VarScan2 (v2.3.7)[14], HaplotypeCaller and UnifiedGenotyper (GATK, v3.3-0)[15,16]. In addition, the pipeline established on the MiSeq Reporter software (v2.4.60) was run in parallel. Variants identified were combined and annotated using ANNOVAR (v2016Feb01)[17]. All programs were executed following the authors' recommendations.

Mass spectrometry analysis

HEK293T cells stably expressing GFP-RPS15^{WT} (2 clones), GFP-RPS15^{P131S} (2 clones) and GFP-RPS15^{S138F} (4 independent clones) in which we had partially (GFP-RPS15^{S138F}) or totally ablated endogenous *RPS15*, or MEC1 cells stably expressing GFP-RPS15^{WT}, GFP-RPS15^{P131S}, GFP-RPS15^{G132S}, GFP-RPS15^{T136A}, GFP-RPS15^{H137Y} and GFP-RPS15^{S138F} (3 independent clones per variant), were lysed in 8 M urea buffer (8 M urea, 50 mM EPPS pH 8.0, 75 mM NaCl, protease and phosphatase inhibitors [Roche]) and protein content was quantified by BCA. Then, disulfide bonds were reduced with 5 mM TCEP for 30 min, alkylated with 14 mM iodoacetamide for 30 min in the dark, and finally quenched with 10 mM DTT for 15 min. 200 µg of protein were precipitated with methanol/chloroform, resuspended in 200 mM EPPS pH 8.5, and digested overnight at room temperature with LysC (1:100, LysC:protein). The day after, trypsin was added (1:75, trypsin:protein) and incubated 5 extra hours at 37 ˚C. After digestion, peptide concentration was calculated using the quantitative colorimetric peptide assay (Pierce) and 25 µg of peptides were labeled with the TMT-10 plex reagents (Pierce) as described previously[18]. A peptide pool (bridge sample) from all 8 (HEK293T clones) or 18 (MEC1 clones) samples was also made by adding an equal amount of each one, and labeled with the last TMT tag (131 m/z). Equal amounts of labeled peptides were combined (10 samples per TMT) and fractionated in a basic pH reverse phase chromatography. All 96 fractions collected were combined into 24, 12 of which were desalted via StageTip and dried down in a SpeedVac. Finally, cleaned peptides were dissolved in 3% formic acid and 3% acetonitrile (ACN), and separated by reversed phase chromatography using a C18 (Accucore 150 2.6 µm) column mounted in a Proxeon EASY-nLC 1000 LC pump (Thermo Fisher) coupled to an Orbitrap Fusion mass spectrometer (Thermo Fisher) in a

SPS-MS3 mode[19]. In the mass spectrometer, MS1 spectra were detected in the Orbitrap (mass range: 350-1400 m/z, 120k resolution, maximum injection time of 100 ms, automatic gain control (AGC) $5x10^5$). Precursors for MS2/MS3 analysis were selected using a TopSpeed of 2 seconds, isolated in the quadrupole with an isolation window of 0.7 m/z, fragmented by CID (normalized collision energy, NCE, of 35%) and detected in the ion trap (AGC $2x10^4$, maximum injection time 150 ms). For TMT quantification, the synchronous-precursor-selection (SPS)-MS3 method was used, where the 10 most intense fragments ions of each MS2, were further isolated, fragmented by HCD (NCE of 65%), and detected in the Orbitrap (50k of resolution, maximum injection time of 250 ms, AGC of $2x10^5$). All raw files obtained from the mass spectrometer were analyzed using in-house software[20] based on SEQUEST. All searches were performed against the human Uniprot database (February 2014), including the decoy reverse database and the most common contaminants. Precursor and product ion tolerances were set up to 20 ppm and 0.9 Da respectively. Carbamidomethylation of cysteines (+57.0215 Da) and TMT labeling (+229.1629 Da) on lysines and peptide N-termini were included as static modifications, and methionine oxidation (+15.9949 Da) as a variable modification. Peptide-spectrum matches (PSMs) were adjusted to a 1% false discovery rate (FDR)[21,22] using a linear discriminant analysis[20]. Moreover, proteins were further collapsed to a final protein-level FDR of 1% and assembled by principles of parsimony to produce the smallest set of proteins necessary to account for all observed peptides. Relative quantification values of each peptide were obtained by subtracting the intensities of the TMT report ions from the MS3 spectra. Only those peptides with a summed signal-to-noise ratio higher than 100 were used for protein quantification. Finally, quantifications were normalized assuming equal protein loading for all ten samples (per TMT) and exported for further analysis in Microsoft Excel and GraphPad Prism 7.0 software. To determine the number of proteins changed as a result of *RPS15* mutations, multiple t-test analyses were performed for each protein across the dataset and corrected for multiple testing using the Bonferroni-Dunn method (adjusted $P<0.05$). Among these, a ratio change threshold of 1.5-fold in protein abundance with respect to GFP-$RPS15^{WT}$-expressing cells was additionally established. Unsupervised hierarchical clustering, heat maps and principal component analysis were generated with Perseus (http://www.coxdocs.org/doku.php?id=perseus:start)[23]. All mass spectrometry proteomics data have been deposited in the ProteomeXchange Consortium via the PRIDE partner repository[24] with the dataset identifier (requested, pending to be received).

Gene set enrichment analysis

To determine possible altered pathways from proteomic data-sets, we performed standard Gene Set Enrichment Analysis (GSEA)[25] using GSEA v3.0 and the gene sets derived from the Reactome database, included within the collection C2 of the Molecular Signatures Database v6.0 (MSigDB v6.0) (http://software.broadinstitute.org/gsea/index.jsp). We used signal-to-noise correlation as the ranking metric and 1000 permutations of gene set to estimate significance. The maximum gene set size was set to 500 genes and the minimum gene set size was set to 15 genes. Selected enriched pathways had a relaxed FDR of <0.25 and P<0.01. Selected enriched gene-sets were analyzed later with the leading edge analysis tool to find the shared subset of up- or down- regulated proteins and to define the main altered biological signatures.

Statistical analysis

Student's t-tests, multiple t-test and one- and two-way ANOVA, were performed using GraphPad Prism 7.0 software. Differences were considered statistically significant when P<0.05 (*P<0.033, **P<0.002, ***P<0.001). The prognostic impact of *RPS15* mutations was evaluated for time to first treatment (TTFT) from the time of sampling, considering disease-unrelated deaths as competing events. Gray's test was used for comparing the cumulative incidence curves of TTFT, while the Fine-Gray multivariate regression model with Backward-stepwise elimination was applied to test the independent prognostic value of *RPS15* mutations on TTFT when considering the IGHV mutational status, genomic aberrations (tri12, del(13q), del(11q), del(17p)/*TP53* mutation), and Binet stage of the patients. Clinical analyses were performed using R (v3.2.4). Results were considered statistically significant when P<0.05 (*P<0.05, **P<0.01, ***P<0.001).

Supplemental References

1. Poulin F, Gingras AC, Olsen H, Chevalier S, Sonenberg N. 4E-BP3, a new member of the eukaryotic initiation factor 4E-binding protein family. *J Biol Chem*. 1998;273(22):14002-14007.

2. Cheng KC, Inglese J. A coincidence reporter-gene system for high-throughput screening. *Nat Methods*. 2012;9(10):937.

3. Kim JH, Lee SR, Li LH, et al. High cleavage efficiency of a 2A peptide derived from porcine teschovirus-1 in human cell lines, zebrafish and mice. *PLoS One*. 2011;6(4):e18556.

4. Salas-Marco J, Bedwell DM. Discrimination between defects in elongation fidelity and termination efficiency provides mechanistic insights into translational readthrough. *J Mol Biol*. 2005;348(4):801-815.

5. Kramer EB, Farabaugh PJ. The frequency of translational misreading errors in E. coli is largely determined by tRNA competition. *RNA*. 2007;13(1):87-96.

6. Branchini BR, Murtiashaw MH, Magyar RA, Anderson SM. The role of lysine 529, a conserved residue of the acyl-adenylate-forming enzyme superfamily, in firefly luciferase. *Biochemistry*. 2000;39(18):5433-5440.

7. Sanjana NE, Shalem O, Zhang F. Improved vectors and genome-wide libraries for CRISPR screening. *Nat Methods*. 2014;11(8):783-784.

8. Puente XS, Bea S, Valdes-Mas R, et al. Non-coding recurrent mutations in chronic lymphocytic leukaemia. *Nature*. 2015;526(7574):519-524.

9. Nadeu F, Delgado J, Royo C, et al. Clinical impact of clonal and subclonal TP53, SF3B1, BIRC3, NOTCH1, and ATM mutations in chronic lymphocytic leukemia. *Blood*. 2016;127(17):2122-2130.

10. Bolger AM, Lohse M, Usadel B. Trimmomatic: a flexible trimmer for Illumina sequence data. *Bioinformatics*. 2014;30(15):2114-2120.

11. Dodt M, Roehr JT, Ahmed R, Dieterich C. FLEXBAR-Flexible Barcode and Adapter Processing for Next-Generation Sequencing Platforms. *Biology (Basel)*. 2012;1(3):895-905.

12. Li H, Durbin R. Fast and accurate short read alignment with Burrows-Wheeler transform. *Bioinformatics*. 2009;25(14):1754-1760.

13. McKenna A, Hanna M, Banks E, et al. The Genome Analysis Toolkit: a MapReduce framework for analyzing next-generation DNA sequencing data. *Genome Res*. 2010;20(9):1297-1303.

14. Koboldt DC, Zhang Q, Larson DE, et al. VarScan 2: somatic mutation and copy number alteration discovery in cancer by exome sequencing. *Genome Res*. 2012;22(3):568-576.

15. Van der Auwera GA, Carneiro MO, Hartl C, et al. From FastQ data to high confidence variant calls: the Genome Analysis Toolkit best practices pipeline. *Curr Protoc Bioinformatics*. 2013;43:11 10 11-33.

16. DePristo MA, Banks E, Poplin R, et al. A framework for variation discovery and genotyping using next-generation DNA sequencing data. *Nat Genet*. 2011;43(5):491-498.

17. Wang K, Li M, Hakonarson H. ANNOVAR: functional annotation of genetic variants from high-throughput sequencing data. *Nucleic Acids Res*. 2010;38(16):e164.

18. Paulo JA, O'Connell JD, Gygi SP. A Triple Knockout (TKO) Proteomics Standard for Diagnosing Ion Interference in Isobaric Labeling Experiments. *J Am Soc Mass Spectrom*. 2016;27(10):1620-1625.

19. McAlister GC, Nusinow DP, Jedrychowski MP, et al. MultiNotch MS3 enables accurate, sensitive, and multiplexed detection of differential expression across cancer cell line proteomes. *Anal Chem*. 2014;86(14):7150-7158.

20. Huttlin EL, Jedrychowski MP, Elias JE, et al. A tissue-specific atlas of mouse protein phosphorylation and expression. *Cell*. 2010;143(7):1174-1189.

21. Elias JE, Gygi SP. Target-decoy search strategy for increased confidence in large-scale protein identifications by mass spectrometry. *Nat Methods*. 2007;4(3):207-214.

22. Elias JE, Gygi SP. Target-decoy search strategy for mass spectrometry-based proteomics. *Methods Mol Biol*. 2010;604:55-71.

23. Tyanova S, Temu T, Sinitcyn P, et al. The Perseus computational platform for comprehensive analysis of (prote)omics data. *Nat Methods*. 2016;13(9):731-740.

24. Vizcaino JA, Csordas A, del-Toro N, et al. 2016 update of the PRIDE database and its related tools. *Nucleic Acids Res*. 2016;44(D1):D447-456.

25. Subramanian A, Tamayo P, Mootha VK, et al. Gene set enrichment analysis: a knowledge-based approach for interpreting genome-wide expression profiles. *Proc Natl Acad Sci U S A*. 2005;102(43):15545-15550.

Supplemental Table 1: Primer pairs used in this work. Chr, chromosome; bp, base pairs; dpt-NGS, deep-targeted next generation sequencing; AS-PCR, Allele specific polymerase chain reaction; qPCR, quantitative PCR; RT-qPCR, reverse transcription quantitative PCR.

Target gene	Target region	Chr	Start position (hg19)	End position (hg19)	Forward primer (5' → 3')	Reverse specific primer (5' → 3')	Amplicon length (bp)	Technique
RPS15	Exon 3	19	1439931	1440129	ACCAAGCCTTAGTTCTCTGTCC	CGCCTCCTTCTTGGCCTTG	199	dpt-NGS
RPS15	Exon 3	19	1440079	1440259	CGGAAGCAGCACTCCCTG	CACACACCTTGATCTCCACCT	181	dpt-NGS
RPS15	Exon 3	19	1440162	1440343	GCACCTGCGGGACATGA	GGGAGACCAAGAGCAAAGCTG	182	dpt-NGS
RPS15	Exon 4	19	1440285	1440467	GCTGGGGTCGCCTGAT	GAGCCATTACTTGAGAGGGATGA	183	dpt-NGS
RPS15	Exon 4	19	1440373	1440571	GCGAGTTCTCCATCACCTACAAG	CTCACACCACGAACCTGAAGC	199	dpt-NGS
RPS15	Exon 4	19	1440439	1440894	CCCGCTTCATCCCTCTCA	GGAGATGAGGGAAGCCAGAA	456	AS-PCR
RPS15^{K145*}	Exon 4	19	1440439	1440894	CCCGCTTCATCCCTCTC**T**	GGAGATGAGGGAAGCCAGAA	456	AS-PCR
ACTB	Exon 5	7	5567668	5567829	ATTTCCCTCTCAGGCATGG	GATCTCCTTCTGCATCCTGTC	162	qPCR
ACTB	Exon1-2	7	5569264	5570204	CACAGAGCCTCGCCTTTGCCGAT	CGAGCGCGGCGATATCATCATCC	81	RT-qPCR
EGFP	Vector	-	-	-	AACCACTACCTGAGCACCCA	CTTGTACAGCTCGTCCATGC	123	RT-qPCR and qPCR

Supplemental Table 2: Antibodies used in this work. IB, immunoblotting; IF, immunofluorescence; IP, immunoprecipitation.

Antibody	Specie and type	Technique and use dilution	Reference
Anti-*β*-actin	Mouse monoclonal	IB →1:2000	Sigma (A5441)
Anti-EF2	Rabbit polyclonal	IB →1:1000	Santa Cruz Biotechnology (SC-25634)
Anti-Flag	Mouse monoclonal	IB →1:1000; IF →1:100	Sigma(F1804)
Anti-GAPDH	Rabbit polyclonal	IB →1:1000	Santa Cruz Biotechnology (SC-25778)
Anti-GFP	Rabbit polyclonal	IB →1:500	Santa Cruz Biotechnology (SC-8334)
Anti-GFP	Rabbit polyclonal	IB →1:1000; IP→2µg	Clontech Laboratories, Inc. (#632592)
Anti-HA	Rat monoclonal	IB →1:500	Roche (3F10)
Anti-PolyUbiquitin	Mouse monoclonal	IB →1:1000	Enzo life sciencies (BML-PW8805)
Anti-RPL11	Rabbit monoclonal	IB →1:1000	Cell Signalling (#14382)
Anti-RPS15	Rabbit monoclonal	IB →1:1000; IF →1:100	Abcam (ab 157193)
Anti-RPS6	Mouse monoclonal	IB →1:1000	Cell Signalling (#2317)
IRDye 680RD secondary antibody	Goat anti mouse	IB →1:10000	Li-COR (926-68070)
IRDye 680RD secondary antibody	Goat anti rabbit	IB →1:10000	Li-COR (926-68071)
IRDye 680RD secondary antibody	Goat anti rat	IB →1:10000	Li-COR (926-68076)
IRDye 800CW secondary antibody	Goat anti mouse	IB →1:10000	Li-COR (926-32210)
IRDye 800CW secondary antibody	Goat anti rabbit	IB →1:10000	Li-COR (926-32211)
Alexa Fluor 546 secondary antibody	Goat anti rabbit	IF →1:500	Invitrogen (#A-11035)

Supplemental Table 3: *RPS15* mutations in the validation cohort of 216 previously untreated CLL patients analyzed by deep-targeted NGS. Ref, reference; Var, variant; VAF, variant allele frequency.

Case	Gene	Somatic criteria[a]	Chr	Genomic position (hg19)	Transcript	Exon	Ref	Var	cDNA	Amino acid	VAF	Mutation type	Verification[b]
108	*RPS15*	Somatic by NGS	chr19	1440429	NM_001018	4	A	G	c.A406G	p.T136A	24.88	Missense	NGS
108	*RPS15*	Somatic by NGS	chr19	1440432	NM_001018	4	C	T	c.C409T	p.H137Y	9.34	Missense	NGS
198	*RPS15*	Somatic by NGS	chr19	1440429	NM_001018	4	A	G	c.A406G	p.T136A	49.61	Missense	NGS
364	*RPS15*	Somatic in COSMICv77 and in custom database	chr19	1440436	NM_001018	4	C	T	c.C413T	p.S138F	1.09	Missense	NGS
521	*RPS15*	Somatic by NGS	chr19	1440415	NM_001018	4	C	G	c.C392G	p.P131R	24.67	Missense	Not done
605	*RPS15*	Truncating	chr19	1440456	NM_001018	4	A	T	c.A433T	p.K145*	43.30	Nonsense	AS-PCR
1357	*RPS15*	Somatic by NGS	chr19	1440426	NM_001018	4	G	A	c.G403A	p.A135T	22.61	Missense	NGS
1381	*RPS15*	Truncating	chr19	1440456	NM_001018	4	A	T	c.A433T	p.K145*	20.96	Nonsense	AS-PCR
1460	*RPS15*	Somatic by NGS	chr19	1440456	NM_001018	4	A	C	c.A433C	p.K145Q	40.89	Missense	Not done

[a]Somatic in COSMICv77, confirmed somatic in at least one sample in COSMIC v77 database; Custom database, confirmed somatic in at least one sample in our custom WGS/WES CLL database; Somatic by NGS, confirmed somatic by targeted-NGS of the normal DNA. Truncating, truncating mutations (frameshift indel, nonsense, or affecting a splice site) were considered somatic.

[b]NGS, verification of the mutation by a second independent round of NGS; AS-PCR, verification done by allele-specific (AS)-PCR; Not done, verification step not performed. Verification not performed in some mutations present at high variant allele frequency (VAF).

Supplemental Table 4: Clinical characteristics of patients with and without *RPS15* mutations.

Parameter	Category	CLL with unmutated *RPS15* (n=656)	CLL with mutated *RPS15* (n=12)	*P*-Value
Gender	% male/female	59/41	58/42	1
Age (years)	Median (range)	67 (19-94)	66 (47-74)	0.170
Binet stage[a]	A	439	7	1
	B	130	3	
	C	54	0	
	Unknown	33	2	
IGHV mutational status[b]	Unmutated	249	11	<0.001
	Mutated	377	0	
	Unknown	30	1	
Copy number alterations	Trisomy 12	97/628 (15.4%)	1/10 (10%)	1
	Deletion 13q	298/628 (47.5%)	3/10 (30%)	0.348
	Deletion 11q	56/628 (8.92%)	0/10 (0%)	1
	Deletion 17p/*TP53* mut	50/630 (7.9%)	0/10 (0%)	1
Patients treated during follow-up[c]	n (%)	338 (51.5)	12 (100)	<0.001
Patients deceased during follow-up[d]	n (%)	177 (27)	4 (33.3)	0.734

IGHV unmutated, ≥98% identity with germ line.

[a]*P* value of the comparison between the number of patients at Binet A vs Binet B/C in both subgroups.
[b]*P* value of the comparison between the number of mutated and unmutated IGHV patients in both subgroups.
[c]*P* value of the comparison of the cumulative incidence curves of TTFT by Gray's test.
[d]*P* value of the comparison of the survival curves by log-rank test.

Supplemental Table 5: Fine-Gray multivariate regression model after Backward-stepwise elimination for time to-first treatment designed to test the independent prognostic value of *RPS15* mutations.

Variable	Hazard ratio (95% CI)	*P*-value
Binet stage (B/C vs. A)	5.06 (3.83-6.69)	< 0.001
IGHV (unmutated vs. mutated)	3.20 (2.42-4.24)	< 0.001
RPS15 (mutated vs. unmutated)	1.77 (1.29-2.43)	< 0.001

Starting model: IGHV (unmutated vs. mutated), Binet stage (B/C vs. A), *RPS15* mutations (mutated at any VAF vs. unmutated), trisomy 12 (presence vs. absence), deletion 13q (presence vs. absence), deletion 11q (presence vs. absence), and deletion 17q and/or *TP53* mutation (presence vs. absence). CI, confidence interval.

Supplemental Table 6: *RPS15* mutations in other tumor types as annotated in COSMIC and c-Bioportal.

Position	Mutation	Exon	Cancer type	Counts	Frequency (%)	Database
6	**p.Q6H**	2	Thyroid	1	0.13	COSMIC
8	**p.K8del**	2	Stomach	1	0.21	c-BioPortal
15	**p.F15L**	2	Adrenal gland	1	0.16	COSMIC
36	**p.L36M**	3	Thyroid	1	0.13	COSMIC
39	**p.A39E**	3	Pancreas	1	0.06	COSMIC
44	**p.R44P**	3	Prostate	1	0.06	COSMIC-cBioPortal
44	**p.R44L**	3	Large intestine	1	0.06	COSMIC
47	**p.R47P**	3	Melanoma	1	2.56	c-BioPortal
51	**p.R51W**	3	Endometrium	1	0.15	COSMIC
53	**p.Q53K**	3	Thyroid	1	0.13	COSMIC
55	**p.S55C**	3	Breast	1	0.12	c-BioPortal
64	**p.K64N**	3	Head and neck	1	0.19	c-BioPortal
67	**p.A67V**	3	Large intestine	1	0.06	COSMIC
79	**p.H79Y**	3	Large intestine	1	0.06	COSMIC
81	**p.R81Q**	3	Lung	1	0.05	COSMIC-cBioPortal
81	**p.R81W**	3	Large intestine	1	0.06	COSMIC
82	**p.D82E**	3	Liver	1	0.05	COSMIC
92	**p.S92I**	3	Endometrium	1	0.15	COSMIC
95	**p.G95D**	3	Liver	1	0.05	COSMIC
99	**p.G99R**	3	Breast	1	0.12	c-BioPortal
104	**p.Q104***	3	Head and neck	1	0.08	COSMIC
117	**p.G117D**	4	Large intestine	1	0.06	COSMIC
123	**p.Y123H**	4	Thyroid	1	0.13	COSMIC
144	**p.L144F**	4	Melanoma	1	0.08	COSMIC

Supplemental Table 7: Significantly enriched (FDR<0.25) gene sets identified by GSEA analysis of proteomic data from GFP-RPS15^{P131S}-expressing HEK293T cells. Red, positively-correlated enriched gene sets (16). Blue, negatively-correlated enriched gene sets (24).

Gene Set	Size	ES	NES	NOM *P*-value	FDR *Q*-value	FWER *P*-value	Rank at Max
REACTOME DNA STRAND ELONGATION	29	0.575	1.944	0	0.113	0.087	1981
REACTOME KINESINS	18	0.642	1.941	0.002	0.057	0.088	805
REACTOME MUSCLE CONTRACTION	21	0.600	1.869	0	0.075	0.166	1598
REACTOME SMOOTH MUSCLE CONTRACTION	15	0.680	1.859	0.006	0.065	0.186	1598
REACTOME SEMA4D INDUCED CELL MIGRATION AND GROWTH CONE COLLAPSE	18	0.609	1.841	0	0.062	0.223	1598
REACTOME MITOTIC G1 G1 S PHASES	107	0.411	1.826	0	0.060	0.256	1242
REACTOME ASSEMBLY OF THE PRE REPLICATIVE COMPLEX	56	0.458	1.801	0	0.066	0.323	1198
REACTOME SEMAPHORIN INTERACTIONS	40	0.481	1.724	0.007	0.120	0.544	1598
REACTOME ACTIVATION OF ATR IN RESPONSE TO REPLICATION STRESS	34	0.486	1.718	0.007	0.111	0.555	1927
REACTOME M G1 TRANSITION	70	0.417	1.676	0	0.140	0.667	1242
REACTOME TRANSCRIPTION COUPLED NER TC NER	37	0.463	1.669	0.006	0.136	0.690	2353
REACTOME G1 S TRANSITION	92	0.382	1.642	0	0.158	0.781	1242
REACTOME FACTORS INVOLVED IN MEGAKARYOCYTE DEVELOPMENT AND PLATELET PRODUCTION	68	0.401	1.639	0	0.149	0.790	1072
REACTOME MITOTIC M G1 PHASES	145	0.349	1.604	0.002	0.183	0.871	1311
REACTOME DNA REPLICATION	161	0.343	1.590	0	0.191	0.906	1311
REACTOME ORC1 REMOVAL FROM CHROMATIN	57	0.399	1.580	0.007	0.192	0.927	1198
REACTOME NONSENSE MEDIATED DECAY ENHANCED BY THE EXON JUNCTION COMPLEX	92	-0.380	-1.582	0.007	0.090	0.929	2293
REACTOME INFLUENZA LIFE CYCLE	121	-0.374	-1.622	0.002	0.067	0.869	2293
REACTOME MITOCHONDRIAL PROTEIN IMPORT	31	-0.498	-1.637	0.009	0.061	0.835	1699
REACTOME TCA CYCLE AND RESPIRATORY ELECTRON TRANSPORT	81	-0.404	-1.643	0.005	0.060	0.807	2250
REACTOME TRANSMEMBRANE TRANSPORT OF SMALL MOLECULES	119	-0.379	-1.644	0.002	0.062	0.801	1223
REACTOME SIGNALING BY HIPPO	16	-0.595	-1.692	0.008	0.045	0.656	124
REACTOME METABOLISM OF PROTEINS	265	-0.356	-1.726	0	0.037	0.552	2293
REACTOME TRANSLATION	127	-0.395	-1.730	0	0.038	0.539	2586
REACTOME CYTOSOLIC TRNA AMINOACYLATION	24	-0.558	-1.733	0.004	0.039	0.522	2300
REACTOME ASSOCIATION OF TRIC CCT WITH TARGET PROTEINS DURING BIOSYNTHESIS	20	-0.585	-1.740	0.008	0.040	0.504	955
REACTOME FORMATION OF TUBULIN FOLDING INTERMEDIATES BY CCT TRIC	15	-0.633	-1.758	0.006	0.035	0.432	532
REACTOME INFLUENZA VIRAL RNA TRANSCRIPTION AND REPLICATION	88	-0.433	-1.759	0	0.037	0.428	2293
REACTOME PEPTIDE CHAIN ELONGATION	74	-0.473	-1.867	0	0.011	0.143	2586
REACTOME ACTIVATION OF THE MRNA UPON BINDING OF THE CAP BINDING COMPLEX AND EIFS	51	-0.512	-1.868	0.002	0.012	0.141	2586
REACTOME SRP DEPENDENT COTRANSLATIONAL PROTEIN TARGETING TO MEMBRANE	91	-0.459	-1.902	0	0.009	0.099	2293
REACTOME PURINE METABOLISM	24	-0.624	-1.930	0	0.006	0.068	2022
REACTOME TRNA AMINOACYLATION	38	-0.542	-1.934	0	0.007	0.063	2300
REACTOME TRANSPORT OF INORGANIC CATIONS ANIONS AND AMINO ACIDS OLIGOPEPTIDES	25	-0.618	-1.945	0.002	0.007	0.056	1067
REACTOME CITRIC ACID CYCLE TCA CYCLE	17	-0.685	-1.980	0	0.004	0.027	1075
REACTOME 3 UTR MEDIATED TRANSLATIONAL REGULATION	94	-0.485	-2.004	0	0.004	0.024	2586
REACTOME SLC MEDIATED TRANSMEMBRANE TRANSPORT	62	-0.525	-2.038	0	0.002	0.010	1085
REACTOME FORMATION OF THE TERNARY COMPLEX AND SUBSEQUENTLY THE 43S COMPLEX	43	-0.583	-2.064	0	0.002	0.007	2586
REACTOME BRANCHED CHAIN AMINO ACID CATABOLISM	16	-0.730	-2.073	0	0.003	0.007	970
REACTOME PYRUVATE METABOLISM AND CITRIC ACID TCA CYCLE	32	-0.638	-2.112	0	0.002	0.002	2048

Supplemental Table 8: Significantly enriched (FDR<0.25) gene sets identified by GSEA analysis of proteomic data from GFP-RPS15^{S138F}-expressing HEK293T cells. Red, positively-correlated enriched gene sets (14). Blue, negatively-correlated enriched gene sets (12).

Gene Set	Size	ES	NES	NOM *P*-value	FDR *Q*-value	FWER *P*-value	Rank at Max
REACTOME DESTABILIZATION OF MRNA BY KSRP	16	0.740	2.109	0	0.010	0.010	863
REACTOME 3 UTR MEDIATED TRANSLATIONAL REGULATION	94	0.480	2.034	0	0.009	0.017	2682
REACTOME PEPTIDE CHAIN ELONGATION	74	0.476	1.930	0	0.029	0.083	2682
REACTOME TRANSPORT OF INORGANIC CATIONS ANIONS AND AMINO ACIDS OLIGOPEPTIDES	25	0.606	1.919	0	0.024	0.090	1024
REACTOME DESTABILIZATION OF MRNA BY TRISTETRAPROLIN TTP	16	0.674	1.885	0	0.028	0.129	1548
REACTOME ACTIVATION OF GENES BY ATF4	17	0.644	1.843	0.002	0.039	0.204	1082
REACTOME SLC MEDIATED TRANSMEMBRANE TRANSPORT	62	0.464	1.825	0	0.040	0.235	1752
REACTOME NONSENSE MEDIATED DECAY ENHANCED BY THE EXON JUNCTION COMPLEX	92	0.432	1.813	0	0.038	0.254	2682
REACTOME TRANSPORT OF RIBONUCLEOPROTEINS INTO THE HOST NUCLEUS	27	0.539	1.772	0.004	0.050	0.358	2012
REACTOME DESTABILIZATION OF MRNA BY BRF1	17	0.608	1.770	0	0.047	0.367	863
REACTOME GLUCOSE TRANSPORT	27	0.528	1.754	0.005	0.046	0.412	2012
REACTOME TRANSPORT OF MATURE MRNA DERIVED FROM AN INTRONLESS TRANSCRIPT	32	0.516	1.751	0	0.044	0.426	2012
REACTOME PI3K AKT ACTIVATION	22	0.559	1.691	0.005	0.056	0.599	1402
REACTOME CYTOSOLIC TRNA AMINOACYLATION	24	0.527	1.667	0.009	0.063	0.683	1968
REACTOME TRANS GOLGI NETWORK VESICLE BUDDING	52	-0.482	-1.697	0	0.086	0.697	67
REACTOME RESPIRATORY ELECTRON TRANSPORT	42	-0.510	-1.719	0.008	0.076	0.618	1885
REACTOME ANTIGEN PRESENTATION FOLDING ASSEMBLY AND PEPTIDE LOADING OF CLASS I MHC	16	-0.658	-1.752	0.004	0.060	0.492	1419
REACTOME BRANCHED CHAIN AMINO ACID CATABOLISM	16	-0.649	-1.825	0	0.032	0.259	1501
REACTOME RESPIRATORY ELECTRON TRANSPORT ATP SYNTHESIS BY CHEMIOSMOTIC COUPLING	51	-0.541	-1.901	0	0.013	0.098	1287
REACTOME INTERFERON GAMMA SIGNALING	21	-0.695	-1.996	0.002	0.003	0.022	780
REACTOME MITOCHONDRIAL PROTEIN IMPORT	31	-0.625	-2.017	0	0.003	0.016	1202
REACTOME LYSOSOME VESICLE BIOGENESIS	20	-0.713	-2.056	0	0.001	0.006	363
REACTOME CHONDROITIN SULFATE DERMATAN SULFATE METABOLISM	16	-0.761	-2.066	0	0.001	0.003	1296
REACTOME PYRUVATE METABOLISM AND CITRIC ACID TCA CYCLE	32	-0.675	-2.172	0	0.000	0.000	858
REACTOME CITRIC ACID CYCLE TCA CYCLE	17	-0.790	-2.197	0	0.000	0.000	858
REACTOME TCA CYCLE AND RESPIRATORY ELECTRON TRANSPORT	81	-0.576	-2.209	0	0.000	0.000	1551

Supplemental Table 9: Significantly enriched (FDR<0.25) gene sets identified by GSEA analysis of proteomic data from GFP-RPS15^{MUT}-expressing MEC1 cells. Red, positively-correlated enriched gene sets (27). Blue, negatively-correlated enriched gene sets (14).

Gene Set	Size	ES	NES	NOM *P*-value	FDR *Q*-value	FWER *P*-value	Rank at Max
REACTOME NONSENSE MEDIATED DECAY ENHANCED BY THE EXON JUNCTION COMPLEX	94	0.553	2.317	0	0.000	0.000	1660
REACTOME 3 UTR MEDIATED TRANSLATIONAL REGULATION	96	0.549	2.281	0	0.000	0.000	1660
REACTOME PEPTIDE CHAIN ELONGATION	76	0.554	2.242	0	0.000	0.001	2296
REACTOME INFLUENZA VIRAL RNA TRANSCRIPTION AND REPLICATION	90	0.536	2.221	0	0.000	0.001	2187
REACTOME INFLUENZA LIFE CYCLE	123	0.462	2.020	0	0.005	0.020	1660
REACTOME METABOLISM OF RNA	231	0.416	1.986	0	0.009	0.043	1788
REACTOME APOPTOTIC EXECUTION PHASE	36	0.569	1.962	0	0.011	0.061	1372
REACTOME ACTIVATION OF THE MRNA UPON BINDING OF THE CAP BINDING COMPLEX AND EIFS AND SUBSEQUENT BINDING TO 43S	54	0.510	1.949	0	0.011	0.071	1559
REACTOME METABOLISM OF MRNA	189	0.420	1.934	0	0.013	0.087	1695
REACTOME LATENT INFECTION OF HOMO SAPIENS WITH MYCOBACTERIUM TUBERCULOSIS	15	0.706	1.931	0.002	0.012	0.089	659
REACTOME FORMATION OF THE TERNARY COMPLEX AND SUBSEQUENTLY THE 43S COMPLEX	46	0.520	1.898	0.002	0.015	0.123	1559
REACTOME DEPOSITION OF NEW CENPA CONTAINING NUCLEOSOMES AT THE CENTROMERE	18	0.646	1.879	0.002	0.017	0.150	596
REACTOME APOPTOTIC CLEAVAGE OF CELLULAR PROTEINS	25	0.578	1.829	0.002	0.026	0.233	1299
REACTOME TRANSLATION	130	0.417	1.823	0	0.026	0.243	1677
REACTOME FORMATION OF TUBULIN FOLDING INTERMEDIATES BY CCT TRIC	17	0.636	1.784	0.004	0.034	0.347	1797
REACTOME MEIOTIC RECOMBINATION	22	0.580	1.784	0.008	0.036	0.345	372
REACTOME PREFOLDIN MEDIATED TRANSFER OF SUBSTRATE TO CCT TRIC	23	0.572	1.782	0.004	0.032	0.356	1332
REACTOME RNA POL I TRANSCRIPTION	24	0.571	1.770	0	0.032	0.407	1123
REACTOME TELOMERE MAINTENANCE	34	0.521	1.770	0.002	0.034	0.404	1294
REACTOME ACTIVATION OF THE PRE REPLICATIVE COMPLEX	22	0.566	1.752	0.006	0.036	0.459	1604
REACTOME DNA STRAND ELONGATION	28	0.513	1.700	0.004	0.052	0.614	1604
REACTOME SRP DEPENDENT COTRANSLATIONAL PROTEIN TARGETING TO MEMBRANE	94	0.400	1.689	0	0.051	0.650	1677
REACTOME CHROMOSOME MAINTENANCE	63	0.425	1.662	0.002	0.063	0.734	1755
REACTOME ANTIVIRAL MECHANISM BY IFN STIMULATED GENES	61	0.422	1.600	0.004	0.097	0.879	1240
REACTOME MITOTIC M M G1 PHASES	139	0.348	1.542	0	0.140	0.960	1788
REACTOME CELL CYCLE	286	0.313	1.527	0	0.144	0.980	1796
REACTOME CELL CYCLE MITOTIC	246	0.305	1.460	0	0.197	0.994	1537
REACTOME POST TRANSLATIONAL PROTEIN MODIFICATION	77	-0.383	-1.538	0.01	0.170	0.973	1622
REACTOME METABOLISM OF AMINO ACIDS AND DERIVATIVES	115	-0.387	-1.653	0	0.082	0.753	1007
REACTOME RESPIRATORY ELECTRON TRANSPORT	56	-0.446	-1.664	0.004	0.080	0.725	2078
REACTOME RESPIRATORY ELECTRON TRANSPORT ATP SYNTHESIS BY CHEMIOSMOTIC COUPLING AND HEAT PRODUCTION BY UNCOUPLING PROTEINS	67	-0.444	-1.740	0	0.041	0.451	1894
REACTOME ANTIGEN PRESENTATION FOLDING ASSEMBLY AND PEPTIDE LOADING OF CLASS I MHC	19	-0.608	-1.775	0.002	0.033	0.359	2101
REACTOME FATTY ACID TRIACYLGLYCEROL AND KETONE BODY METABOLISM	94	-0.443	-1.823	0	0.021	0.231	1465
REACTOME PHOSPHOLIPID METABOLISM	91	-0.460	-1.885	0	0.012	0.129	934
REACTOME METABOLISM OF LIPIDS AND LIPOPROTEINS	220	-0.407	-1.898	0	0.012	0.113	646
REACTOME PYRUVATE METABOLISM AND CITRIC ACID TCA CYCLE	34	-0.588	-1.968	0	0.006	0.045	1107
REACTOME TCA CYCLE AND RESPIRATORY ELECTRON TRANSPORT	97	-0.476	-1.971	0	0.006	0.042	1660
REACTOME CHOLESTEROL BIOSYNTHESIS	17	-0.747	-2.088	0	0.002	0.009	622
REACTOME CITRIC ACID CYCLE TCA CYCLE	19	-0.756	-2.207	0	0.000	0.000	968
REACTOME GLYCEROPHOSPHOLIPID BIOSYNTHESIS	28	-0.699	-2.224	0	0.000	0.000	730
REACTOME TRIGLYCERIDE BIOSYNTHESIS	22	-0.758	-2.321	0	0.000	0.000	588

Supplemental Figure 1

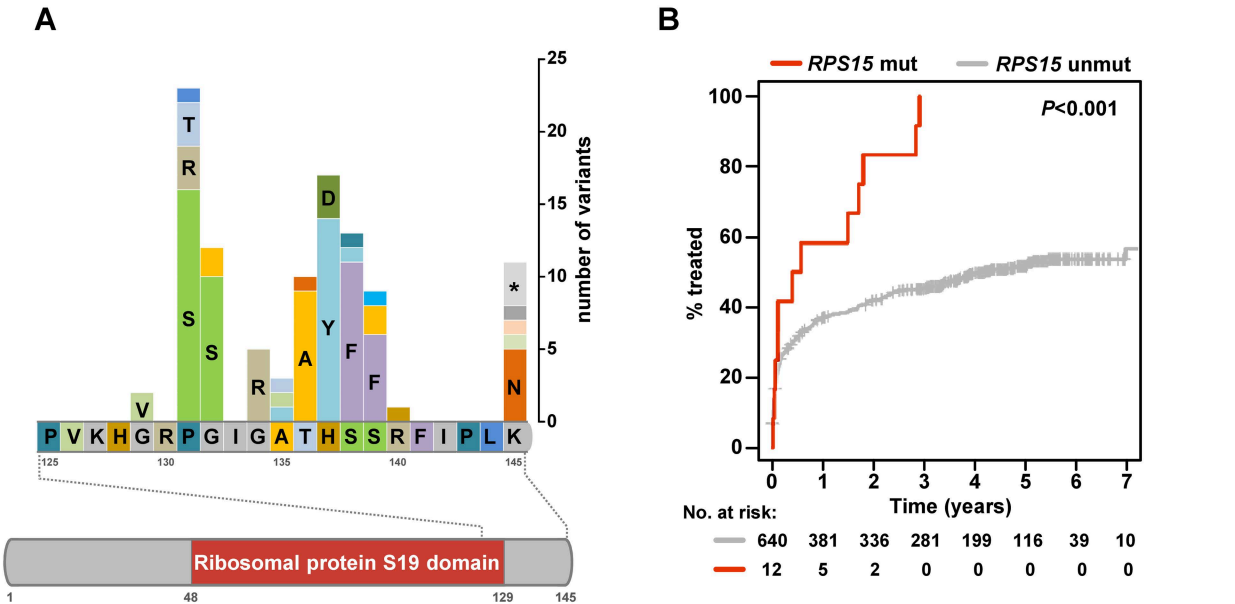

Supplemental Figure 1. Distribution and clinical impact of the C-terminal mutations in RPS15. (A) Schematic representation of RPS15 protein and number and distribution of somatic RPS15 mutations identified in CLL-WES and -WGS studies. Most of the mutations (~85%) clustered to a small C-terminal segment of 9 amino acids (positions 131 to 139). Color-coding indicates the type of amino acid change. *, premature stop codon. (B) Comparison of time to first treatment among CLL patients (Puente et al. 2015 and validation cohorts) harboring an unmutated RPS15 (gray line) vs patients with mutated RPS15 (orange line). P, P-values by Gray's test.

Supplemental Figure 2

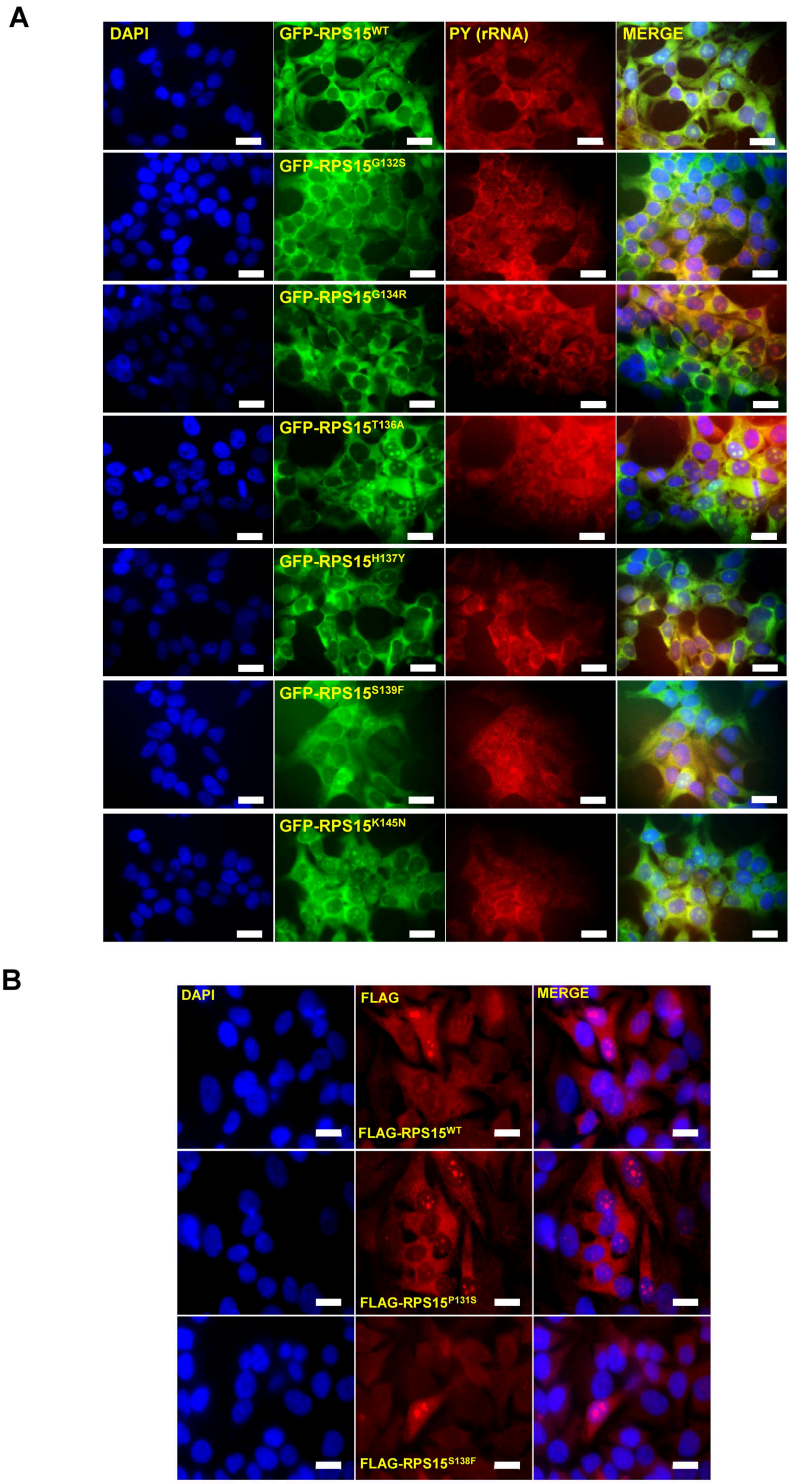

Supplemental Figure 2. *RPS15* recurrent mutations do not alter subcellular distribution on protein. (A) Distribution of RPS15 proteins (wild-type and G132S, G134R, T136A, H137Y, S139F and K145N mutants) fused to GFP in HEK293T cells. rRNA distribution was stained with the RNA-binding dye Pyronin Y (PY). Co-localization is shown in merge panels. Scale bar, 20 µm. (B) Immunofluorescence analysis of FLAG-tagged RPS15^{WT}, RPS15^{P131S} and RPS15^{S138F} mutants in HeLa cells. Both mutants (FLAG-RPS15^{P131S} and FLAG-RPS15^{S138F}) show the same distribution than FLAG-RPS15^{WT}. DAPI staining show nuclei. Scale bar, 20µm.

Supplemental Figure 3

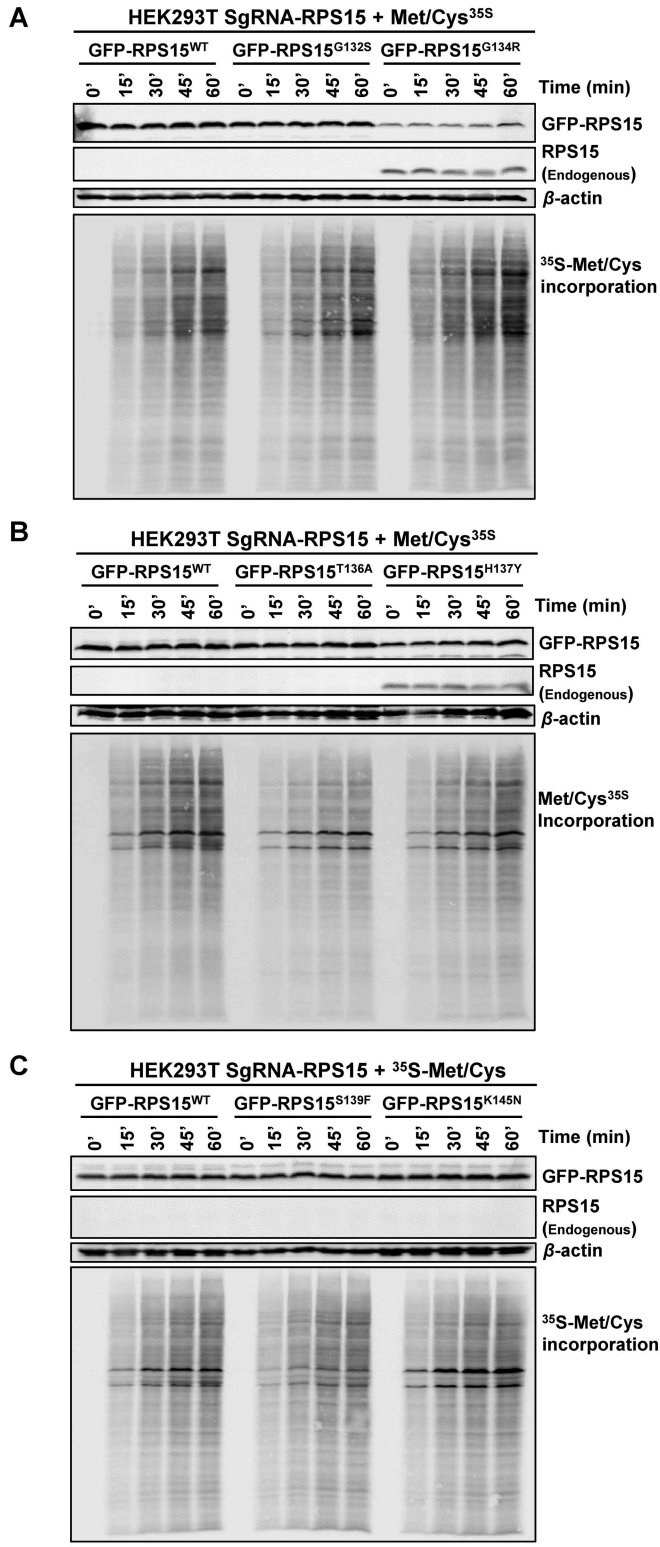

Supplemental figure 3. De novo protein synthesis measured by 35S-Met/Cys incorporation in different GFP-RPS15 mutants. (A) Comparative analysis between GFP-RPS15^{WT}, GFP-RPS15^{G132S} and GFP-RPS15^{G134R}. (B) Comparative analysis between GFP-RPS15^{WT}, GFP-RPS15^{T136A} and GFP-RPS15^{H137Y}. (C) Comparative analysis between GFP-RPS15^{WT}, GFP-RPS15^{S139F} and GFP-RPS15^{K145N}. (A-C) A representative autoradiography image and the associated RPS15 and β-actin immunoblots are shown of 3 independent experiments. Western blot against β-actin was used as loading control.

Supplemental Figure 4

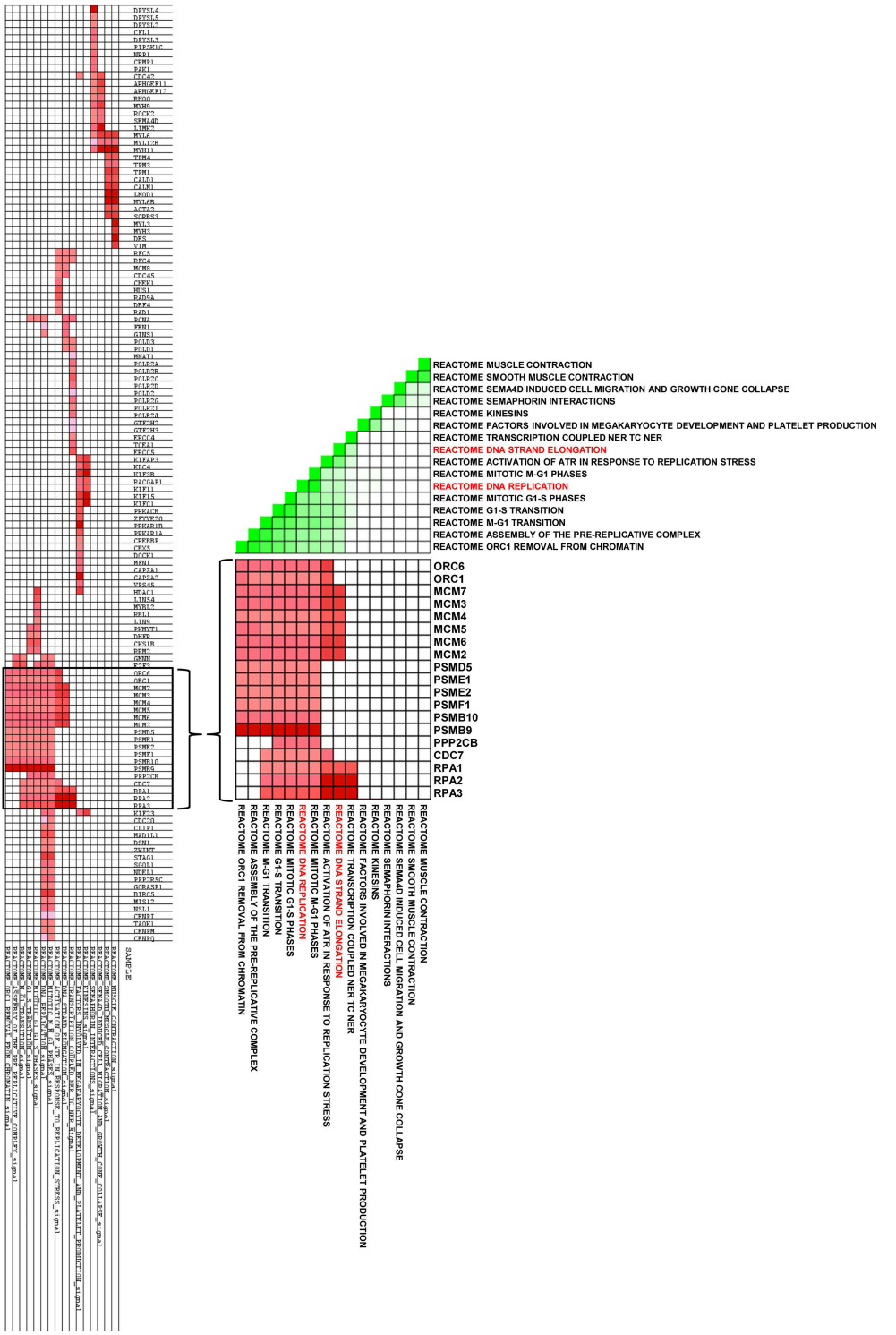

Supplemental Figure 4. Leading edge analysis of positively-correlated enriched gene sets for GFP-RPS15^{P131S} phenotype identifies DNA replication and DNA strand elongation as the main biological signature up-regulated in HEK293T cells. Significantly enriched gene sets at nominal *P*<0.01 and FDR<0.25 (left) shared several components of the DNA replication machinery, coloured in red (right, magnified box).

Supplemental Figure 5

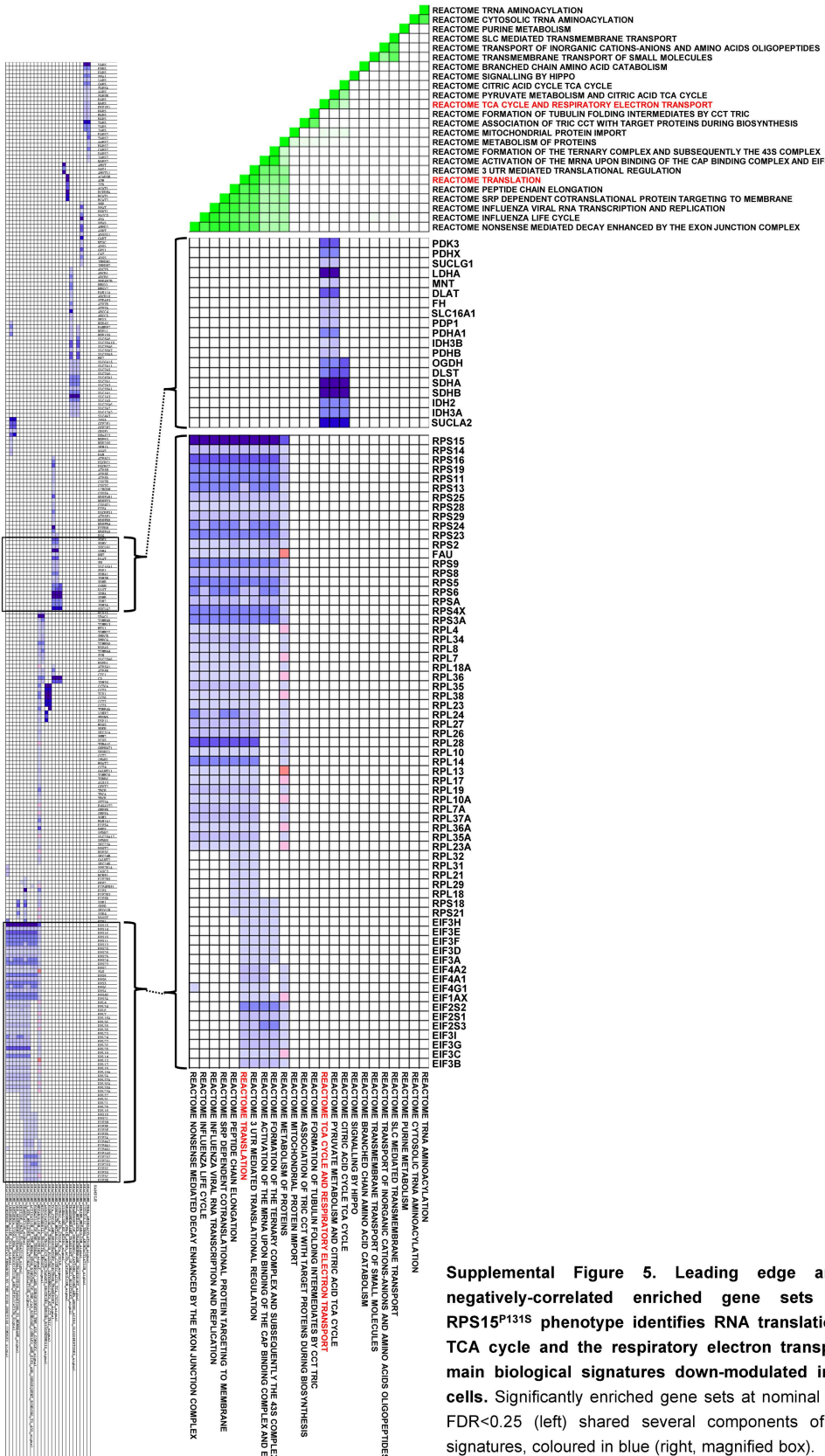

Supplemental Figure 5. Leading edge analysis of negatively-correlated enriched gene sets for GFP-RPS15^{P131S} phenotype identifies RNA translation and the TCA cycle and the respiratory electron transport as the main biological signatures down-modulated in HEK293T cells. Significantly enriched gene sets at nominal P<0.01 and FDR<0.25 (left) shared several components of these two signatures, coloured in blue (right, magnified box).

Supplemental Figure 6

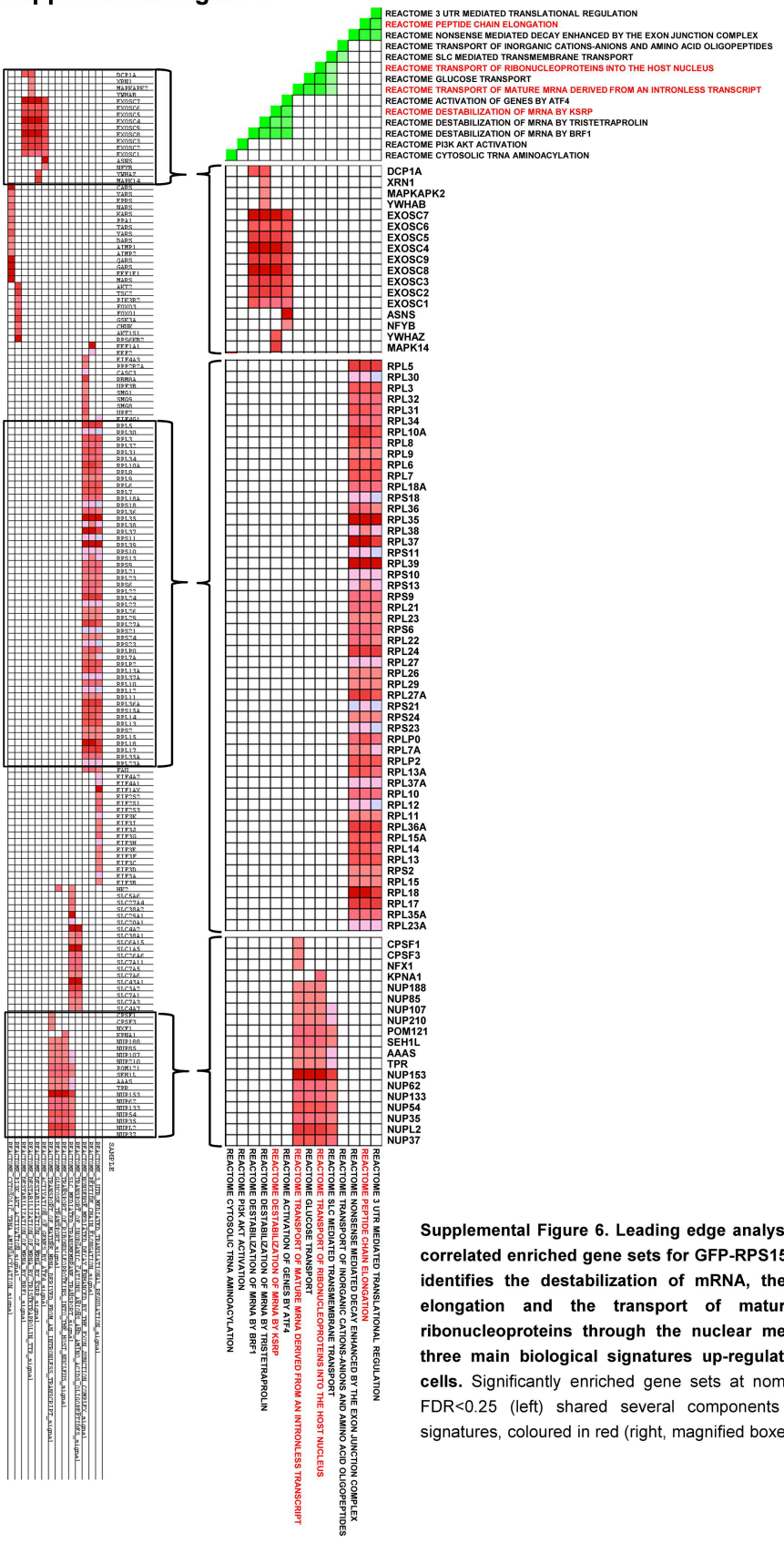

Supplemental Figure 6. Leading edge analysis of positively-correlated enriched gene sets for GFP-RPS15^{S138F} phenotype identifies the destabilization of mRNA, the peptide chain elongation and the transport of mature mRNA and ribonucleoproteins through the nuclear membrane as the three main biological signatures up-regulated in HEK293T cells. Significantly enriched gene sets at nominal *P*<0.01 and FDR<0.25 (left) shared several components of these three signatures, coloured in red (right, magnified boxes).

Supplemental Figure 7

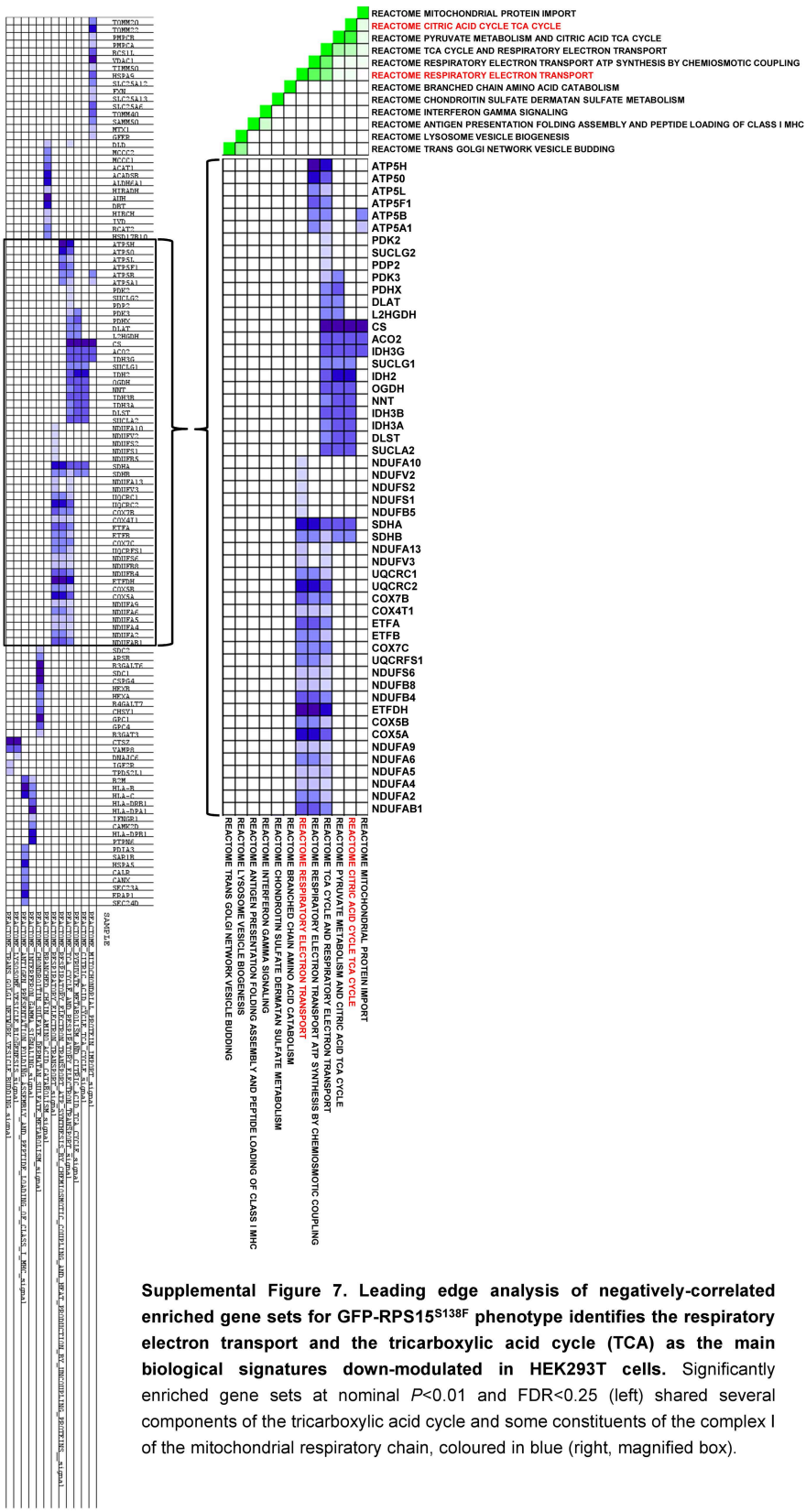

Supplemental Figure 7. Leading edge analysis of negatively-correlated enriched gene sets for GFP-RPS15^{S138F} phenotype identifies the respiratory electron transport and the tricarboxylic acid cycle (TCA) as the main biological signatures down-modulated in HEK293T cells. Significantly enriched gene sets at nominal *P*<0.01 and FDR<0.25 (left) shared several components of the tricarboxylic acid cycle and some constituents of the complex I of the mitochondrial respiratory chain, coloured in blue (right, magnified box).

Supplemental Figure 8

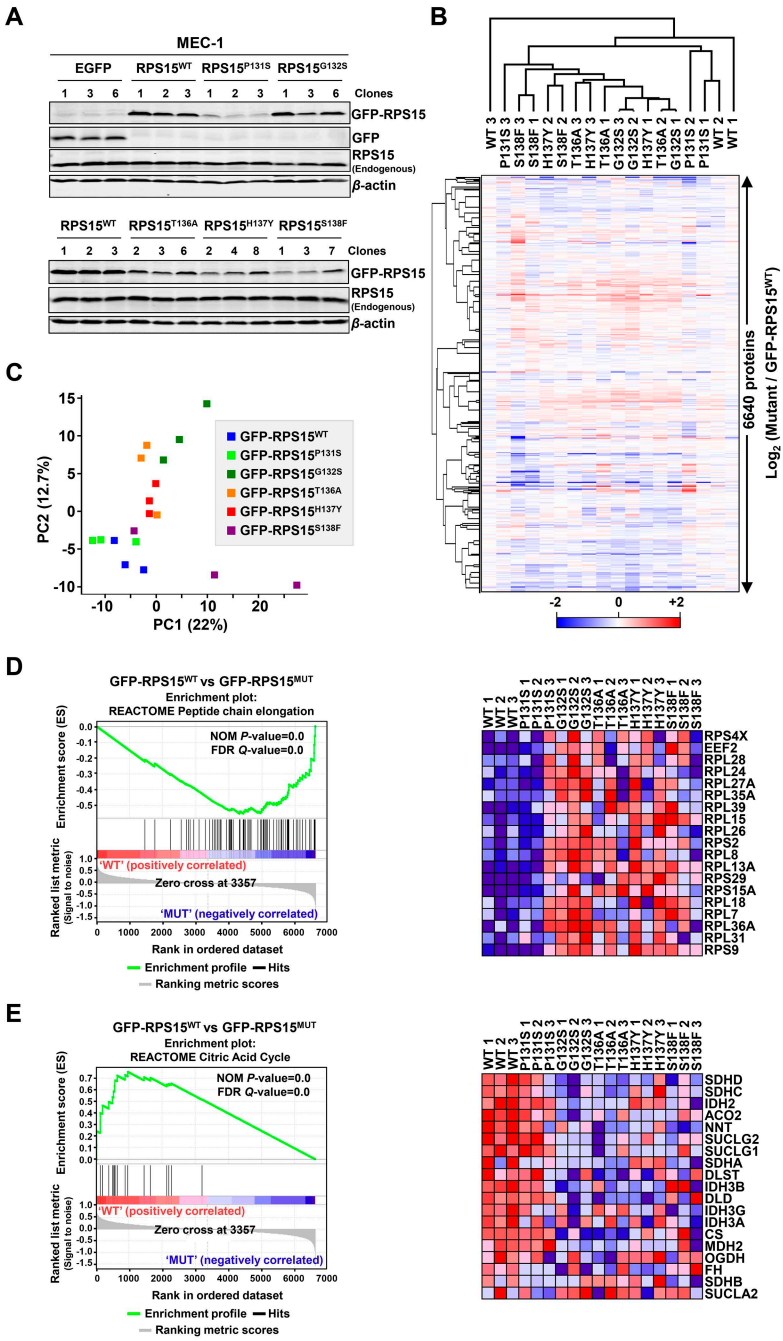

Supplemental Figure 8. RPS15 mutant proteins alter global cell proteome in MEC-1 cells. (A) MEC-1 cells stably expressing the different RPS15 constructs (WT, P131S, G132S, T136A, H137Y and S138F) used for the proteomic analysis. Selected subclones were subjected to western blot analysis with antibodies against GFP, RPS15 and *β*-actin as loading control. (B) Heat-map depicting unsupervised hierarchical clustering of the 18 proteomes analyzed using the total set of proteins identified. Protein abundance is shown as the Log2 ratio between each sample with respect to the average of reference sample (GFP-RPS15^{WT}-expressing MEC-1 cells). (C) Principal component analysis of the relative protein abundances of all 18 proteomes analyzed. (D-E) Comparison of proteomic profiles from GFP-RPS15^{WT} versus GFP-RPS15^{MUT}-expressing MEC-1 cells performed through GSEA. (D) The enrichment plot shown corresponds to peptide chain elongation in the REACTOME database. Right, Heat-map showing the 19 top genes of the GFP-RPS15^{WT} negatively-correlated enriched gene set. (E) The enrichment score plot shown corresponds to citric acid cycle in the REACTOME database. Right, heat-map showing the 19 top genes of the GFP-RPS15^{WT} positively-correlated enriched gene set.

Supplemental Figure 9

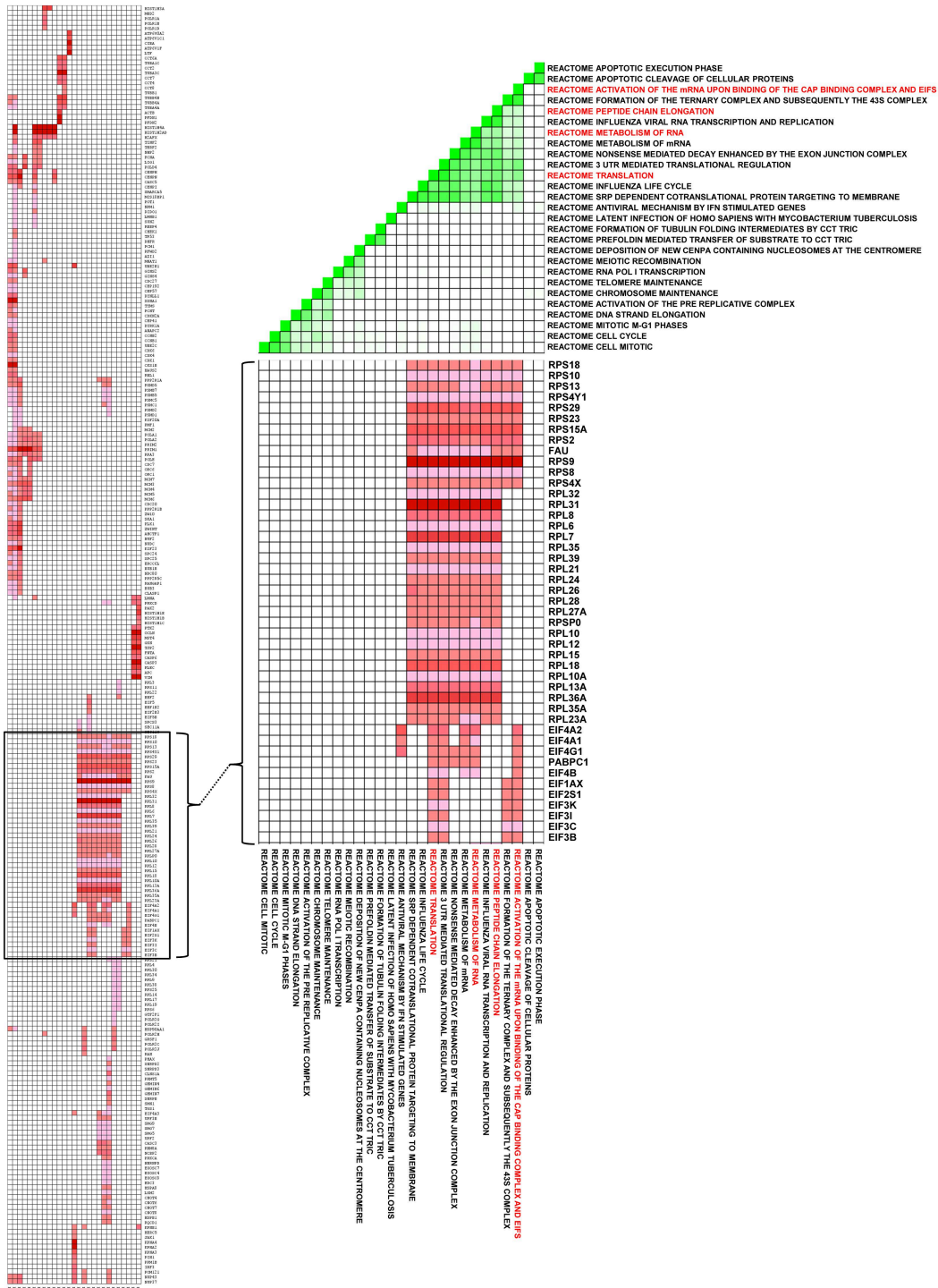

Supplemental Figure 9. Leading edge analysis of positively-correlated enriched gene sets for GFP-RPS15^{MUT} phenotype identifies RNA translation as the main biological signature up-regulated in MEC-1 cells. Significantly enriched gene sets at nominal *P*<0.01 and FDR<0.25 (left) shared several components of the ribosomal 40S and 60S subunits and some eukaryotic initiation factors, coloured in red (right, magnified box).

Supplemental Figure 10

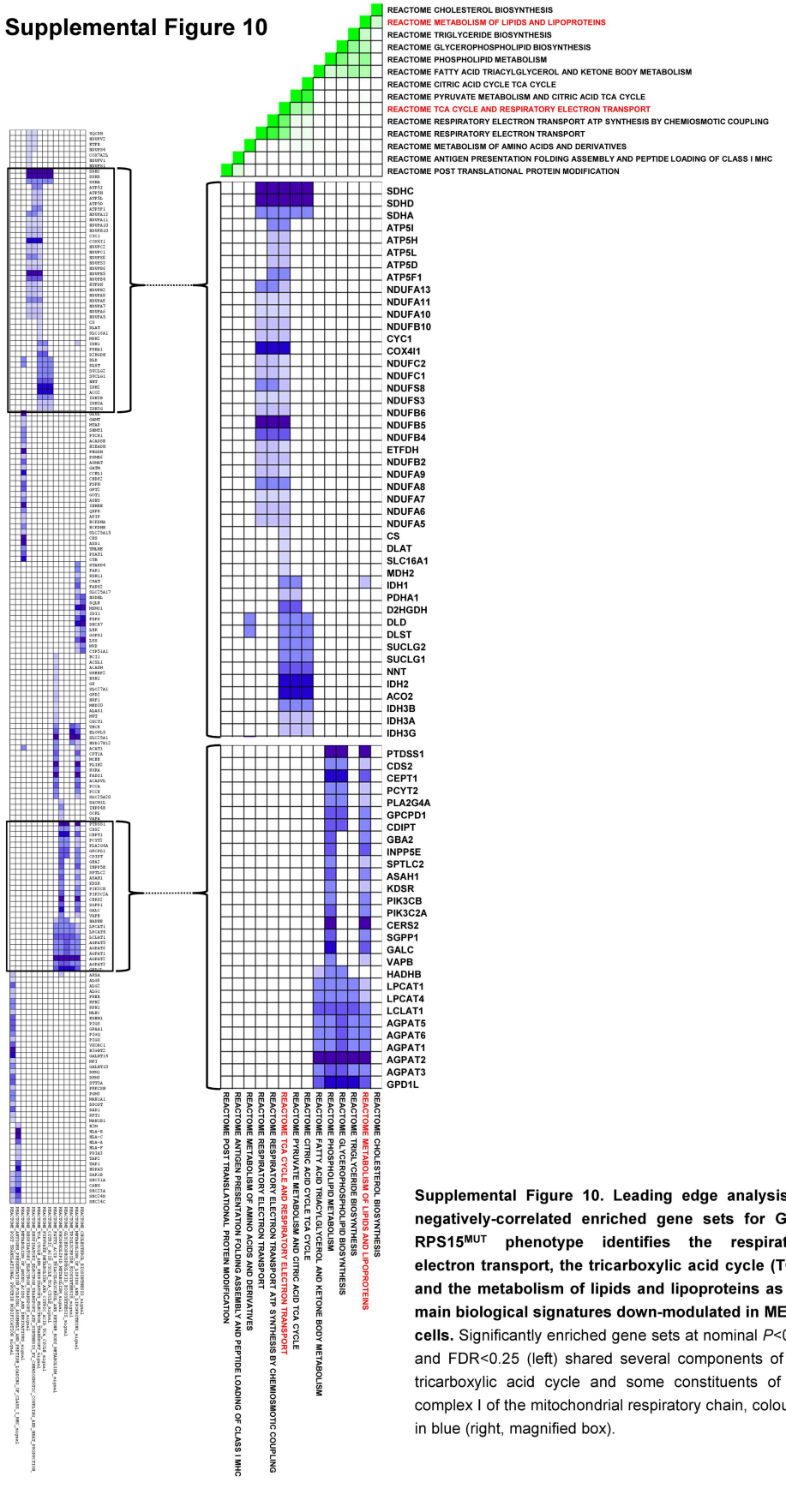

Supplemental Figure 10. Leading edge analysis of negatively-correlated enriched gene sets for GFP-RPS15^{MUT} phenotype identifies the respiratory electron transport, the tricarboxylic acid cycle (TCA) and the metabolism of lipids and lipoproteins as the main biological signatures down-modulated in MEC-1 cells. Significantly enriched gene sets at nominal P<0.01 and FDR<0.25 (left) shared several components of the tricarboxylic acid cycle and some constituents of the complex I of the mitochondrial respiratory chain, coloured in blue (right, magnified box).